

Efficient passivation and low resistivity for p⁺- Si/TiO₂ contact by atomic layer deposition

Naeimeh Mozaffari^{§,*}, *Heping Shen*[§], *Yanting Yin*^{ℳ,‡}, *Yueliang Li*^ℳ, *Daniel Hiller*[§], *Daniel A. Jacobs*[§], *Hieu T. Nguyen*[§], *Pheng Phang*[§], *Gunther G. Andersson*^{ℳ,‡}, *Ute Kaiser*^ℳ, *Thomas P. White*[§], *Klaus Weber*[§], *Kylie R. Catchpole*^{§,*}

[§] Research School of Electrical, Energy and Materials Engineering, The Australian National University, Canberra 2601, Australia

^ℳ Flinders Institute for Nanoscale Science and Technology, Flinders University, Adelaide SA 5042, Australia

[‡] Flinders Microscopy and Microanalysis, College of Science and Engineering, Flinders University, Adelaide, SA 5042, Australia

^ℳ Central Facility of Electron Microscopy, Electron Microscopy Group of Materials Science, Ulm University, Albert-Einstein-Allee 11, 89081 Ulm, Germany

Keywords: Surface passivation, Boron doped silicon, Titanium oxide, forming gas (FG), lifetime

ABSTRACT

The monolithic, two-terminal (2-T) perovskite/silicon tandem solar cell is a promising candidate to increase the power conversion efficiency beyond the theoretical limit of 29.4% for crystalline silicon solar cells. To achieve a high-efficiency 2-T tandem, it is critical to have an interface that can connect the bottom and top sub cells together so that both efficient passivation and good electrical contact are achieved. The majority of works done to date in this area, applied an intermediate layer as the recombination layer between perovskite and silicon, which incurs higher manufacturing costs and an additional processing step. Here we demonstrate a unique and straightforward interlayer-free approach to passivating highly boron-doped low resistivity n-Si using a thin layer of TiO₂ fabricated by atomic layer deposition (ALD) and a suitable pre-treatment of the silicon surface. The passivation of this film is found to be superior to that of thermally-grown SiO₂ formed at high temperatures over 700⁰C. The TiO_x layer leads to a sufficiently low contact resistance of 0.45 Ω.cm² and high quality passivation with a recombination current density (J₀) of 152 fA/cm². The structure is applicable to both perovskite/Si tandems & single-junction Si solar cells.

1. Introduction

Two of the most crucial tasks that the photovoltaic industry is currently focusing on are increasing the module power conversion efficiency (PCE) and decreasing the production costs in order to diminish the cost/watt.¹ One of the main factors to enhance solar cell performance is improving surface passivation, which can be achieved by depletion of minority carriers from the surface and/or reducing density of interface states.^{2,3} Two major techniques have been developed to passivate the surfaces of silicon (Si) cells: chemical passivation⁴ and field effect (or charge-

induced) passivation.⁵ In the former process, the film adheres to dangling bonds of Si and makes them electrically inactive, while the latter involves repelling either holes or electrons by a large net charge in the passivation layer. Excellent passivation can be achieved through a combination of both the aforementioned methods.⁶ Apart from surface passivation, a low contact resistance is essential for achieving high efficiencies. There are two types of contact in current cell structures in industry, of which one is localized contact⁷ and the other one is full-area carrier selective contact.^{8,9} Localized contact structures can require complex and expensive patterning processes such as photolithography, which are not only very costly but also can introduce new contamination on the surface as a result of photoresist residue as well.¹⁰ A carrier selective contact (CSC) is a contact that extracts just one type of charge carrier (hole or electron), so that majority carriers can be transported efficiently and minority carrier recombination can be reduced. A CSC layer can provide superb surface passivation leading to an improvement in open-circuit voltage (V_{oc}), and fill factor (FF). Thus, by eliminating the need for localized doping and opening the contact, a simplified and flexible fabrication process can be achieved.

Having a passivation layer that can also provide good contact is particularly beneficial for two-terminal (2-T) tandem solar cells, where a low band gap bottom cell (e.g. silicon) is serially connected to a high band gap top cell (e.g. perovskite). Generally, the 2-T configuration requires an interlayer between the bottom and top subcells to facilitate the current flow of photogenerated carriers.¹¹ The aforementioned interlayer should have both low electrical and optical losses with easy fabrication processing.¹² Recently, a type of unconventional perovskite/Si tandem structure that bypasses the use of an interlayer was developed,^{12,13} with the advantage of not only reducing the fabrication steps but also eliminating the optical losses associated with highly doped recombination layers. Tandem cell efficiencies >24% were achieved by applying this new concept

to heterojunction Si subcells, while efficiencies approaching 23% were demonstrated with a Si homojunction subcell. Tandem cells based on homojunction Si technology are potentially most relevant to the PV industry given their dominance in commercial products.¹⁴ This interlayer-free design relies on a surprisingly low ohmic contact resistance between p⁺-Si/TiO₂, which enables in-situ recombination on the atomic layer between p⁺-Si and TiO₂. In our previous results, the processing conditions required to achieve a low resistivity p⁺-Si/TiO₂ contact provided only limited surface passivation of the p⁺-Si. This correspondingly induced a high recombination rate in the front emitter of the bottom Si solar cell, thus limiting its contribution to the tandem efficiency. As discussed above, high-efficiency solar cells require interfaces that provide both low contact resistance and excellent surface passivation, which is the focus of this work.

Passivation of a p⁺-emitter on a n-type Si wafer diffused with boron tribromide (BBr₃) is challenging¹⁵ owing to high boron solubility and high concentration of built-in positive charges¹⁶, and development of a low-cost technique to passivate p⁺ emitters is still demanded by industry.¹⁷ Negatively charged dielectric layers are normally favoured options to passivate these surfaces,¹⁶ as they can provide an electric field that repels the minority electrons from the interface and thus suppress recombination.⁶ Various methods have been used to passivate boron-diffused surfaces, such as hydrogenated amorphous silicon (a-Si:H),¹⁸ thermally grown¹⁹ or chemically grown SiO₂¹⁷, Al₂O₃,¹⁶ TiO₂,^{10,20} hafnium oxide,²¹ tantalum oxide,²² and gallium oxide²³ deposited by atomic layer deposition (ALD), plasma-enhanced chemical vapor deposition (PECVD) of SiO_x/SiN_y stacks⁶ or AlO_x,²⁴ sputtered aluminium nitride,²⁵ and stacks of Al₂O₃/SiN_x.²⁶ Although because of the insulating nature of some of the abovementioned materials, it makes it necessary to have the contact opening in the structure. Due to its small conduction band offset with silicon,²⁷ insignificant extinction coefficient, negligible parasitic light absorption, and very low surface

recombination velocities accompanied by low contact resistances, TiO₂ has drawn significant attention as an electron selective contact²⁸ for Si solar cells, which has the potential to lift crystalline Si solar cell efficiency to over 26%.³ Other attractive features of TiO₂ as a CSC are low-cost and non-toxic processing options via atomic layer deposition, thermal evaporation or spin-coating.²⁸ Yang et al. demonstrated surface passivation using an ultrathin SiO₂/TiO₂ stack for the rear side of undiffused n-type silicon solar cell.¹⁰ They reported low contact resistance of 0.02 Ω.cm² with surface recombination velocity of 16 cm/s for 2.5 nm titanium oxide deposited by ALD at 75°C. Cui et al. studied surface passivation of boron diffused 100 Ω cm n-type FZ silicon wafers (with sheet resistance of 120 Ω/sq) using ALD TiO₂ deposited at 75°C.²⁰ They found that increasing the thickness of TiO₂ to around 15 nm improved the passivation to a J₀ of 19 fA/cm² and this value remained almost constant for thicker films. In contrast to these two previous works, and based on our previous work¹² which showed that lowering the boron doping will largely increase the contact resistivity, here we focus on passivation of heavily boron doped silicon to improve the electrical contact, which is more challenging as mentioned above. As we intend to improve the front side passivation of silicon solar cells for future application in 2T tandem cells, the importance of surface passivation outweighs the contact resistance, which led us to choose thicker TiO_x films. In addition, for tandem solar cells, a low temperature process (≤ 200°C for heterojunction and ≤ 400°C for homojunction silicon subcell⁷) is desirable to minimise damage to the bottom silicon cell,¹³ which motivated us towards finding a fabrication method compatible with relatively low temperatures.

In this context, we focus on improving the interface of p⁺-Si/TiO₂ by controlling the fabrication conditions as well as implementing pre-treatment and post-treatment, with the aim of achieving effective surface passivation of heavily boron doped silicon and low contact resistance

simultaneously. There are various methods for TiO₂ deposition such as evaporation,²⁹ spray hydrolysis,³⁰ sol-gel,³¹ sputtering,³² atmospheric pressure chemical vapour deposition (APCVD)³³ and, recently, ALD.^{20,34} Here, we selected ALD to deposit the TiO₂ film, as it can offer high surface uniformity and controlled growth rate at the atomic scale by exploiting sequential, self-limiting reactions between gaseous precursors and the substrate. Consequently, outstanding conformal and uniform films can be obtained on a range of surfaces with precise thickness in the range of angstroms.^{35,36} We developed a novel, cost-effective method to improve the passivation of TiO₂ films on heavily boron-doped surfaces of n-type crystalline Si solar cells using a combination of forming gas (FG) pre-heat treatment of Si substrate followed by ALD deposition of ultrathin TiO₂ at 200°C. An important advantage of this approach is that it can be applied to the interface layer between p⁺-Si and TiO₂ in a perovskite-silicon tandem without the need for an additional recombination layer. The FG annealing of the boron doped silicon substrate prior to subsequent depositions, is a straightforward, relatively low temperature process which improved the ligand exchange and bond formation between silicon and TiO₂. Our results show that FG annealing can reduce recombination by a factor of three at a TiO₂ deposition temperature of 200°C, while also providing acceptably low contact resistance. We note that the work here is not only appropriate for use in 2T silicon-perovskite tandem solar cells, but also for single-junction silicon solar cells.

2. Experimental Section

Surface passivation was investigated on, 5 Ω.cm n-type float-zone (FZ) crystalline silicon (c-Si) with a thickness of 400 μm and 2.5 Ω.cm p-type FZ c-Si wafers with a thickness of 300 μm, with and without boron (p⁺) and phosphorus (n⁺) diffusion. Samples for contact resistance investigation

were fabricated on boron-diffused p-type Czochralski (Cz) c-Si ($1 \Omega \text{ cm}$) wafers with a thickness of $250 \mu\text{m}$.

Initially all wafers were etched in 25wt% Tetramethylammonium hydroxide (TMAH) at approximately 80°C for 5 minutes to remove any saw damage followed by a standard RCA (Radio Corporation of America) cleaning process³⁷ and a 1% w/v HF (hydrofluoric acid) solution dip. Boron and phosphorus diffusion processes were carried out in quartz tube furnaces using liquid BBr_3 and POCl_3 precursors, at 980°C and 900°C , respectively. Four-point probe measurements gave sheet resistances of $23\Omega/\text{sq}$ for boron-diffused and $13.6\Omega/\text{sq}$ for phosphorous-diffused samples, corresponding to surface doping concentrations $7 \times 10^{19} \text{cm}^{-3}$ and $2 \times 10^{20} \text{cm}^{-3}$, respectively. The resultant borosilicate and phosphosilicate glasses layers were then removed using an HF dip process. Another RCA cleaning and HF dip were applied on the wafers prior to pre-heat treatment and ALD- TiO_2 deposition.

Various pre-heat treatment procedures (under high or low temperature) were conducted prior to TiO_2 deposition and their passivation effects were compared. Different types of atmosphere were utilized comprising annealing in FG, N_2 , and O_2 at 400°C for 30 minutes for the low temperature procedure and annealing in O_2 at 700°C for 3 minutes for the high temperature process. For some samples we directly deposited TiO_2 without any pre-heat treatment.

TiO_2 deposition by a thermal ALD system (TFS200, BENEQ) was carried out using titanium tetrachloride (TiCl_4) as the titanium precursor, deionized water as the oxidant agent and pure nitrogen (N_2) as the purge gas. The reactor temperature was initially set to be 230°C , but by decreasing the temperature to 200°C , the minority carrier lifetime improved from around $900\mu\text{s}$ to $1142 \mu\text{s}$ at a carrier density of $1.0\text{E}+15 \text{cm}^{-3}$. At this stage 200°C was chosen as the main deposition temperature for further study, however lower temperatures (including 75°C , 100°C , and 150°C)

were examined as well. The deposition process consisted of 200 sccm (standard cubic centimetres per minute) $N_2(g)$ flow, with a 0.05-s pulses of $TiCl_4$ followed by a 0.05-s pulses of H_2O per cycle, and a 0.75-s purge under a constant flow (300 sccm) of $N_2(g)$ between each precursor pulse. For a deposition temperature of $75^\circ C$, a deposition rate $\sim 0.76 \text{ \AA/cycle}$ was measured by spectroscopic ellipsometry (M2000, J.A. Woolam).

The surface passivation behaviour was studied using a Sinton Instruments WCT-120 photoconductance tool in the transient mode which is not dependent on the optical properties of the sample³⁸. The recombination current density was extracted at $\Delta n = 3.0E+15 \text{ cm}^{-3}$, considering the radiative recombination model of Nguyen³⁹ at 300 K. The electrical contact resistance was evaluated by the Cox and Strack method⁴⁰, in which TiO_2 was deposited on the front side of a double side boron diffused wafer. Subsequently, an array of Al circles with various diameters (0.1, 0.15, 0.2, 0.25, 0.3, 0.35, 0.4, 0.5, 0.6, 0.7, and 0.8 cm) were evaporated on the front side via a shadow mask. The back side of the wafer was coated completely with an Al film. Current-voltage (I-V) measurements at room temperature were performed, which utilized a spreading resistance model to fit the resistance versus diameter data. This method calculates the contact resistance that includes the contact resistance of the metal oxide/Al, the bulk oxide, and the p^+ Si/ oxide.

High-resolution transmission electron microscopy (HRTEM) was used to observe the existence of the interlayer between silicon and TiO_2 , as well as measuring the thickness of these layers accurately. Cross-sectional TEM samples were prepared using standard techniques including grounding, dimpling and ion milling. High-resolution TEM imaging was performed using FEI Titan 80-300 microscope with an image-side C_s -corrector. Additionally, XPS and UPS measurements were individually conducted to determine the elemental composition and electronic structure of different samples. XPS measurements were performed by recording the electrons

emitted due to X-ray radiation from the core level of element with a pass energy of 10 eV in ultrahigh vacuum chamber, which provides information on the chemical composition and valence electron states of the samples. The instrument is described in detail in reference ⁴¹. Calibration of the XP spectra was not applied because no charging was observed during the measurement and the C-C bond of TiO₂ samples was found close to 285.0 eV which is the energy usually applied for calibration of XP spectra. Not applying the calibration procedure allows for identifying chemical changes of C⁴². An error bar for the peak fitting of XPS is normally under ± 0.2 eV, depending on the counts and fitting.

UPS was conducted for acquiring information of work function (WF) and valence electron states. The samples were transferred to the measurement chamber, where a short heating process under vacuum conditions at 250°C for sintered samples and 150°C for un-sintered samples was applied prior to the measurement, to remove the potential moisture and minimize the carbon contamination. The error bar for the electronic properties from UPS is ± 0.1 eV.

Low-temperature PL spectroscopy was performed with a diode-pumped solid-state (DPSS) continuous-wave 532 nm laser to confirm the surface passivation results. The emitted PL signal was captured with an InGaAs array detector. The sample temperature was controlled with a liquid-nitrogen cooled THMS600 Linkam stage. The spectral response of the entire system was determined with a calibrated halogen–tungsten light source.

Grazing incidence X-ray diffraction (GIXRD) analyses were conducted on thin films using a PANalytical X'Pert Pro system, with a tube voltage of 30 kV and a tube current of 10mA to generate copper K _{α} x-rays.

3. Results and Discussion

3.1. Surface passivation and contact resistance

The passivation effect can be studied by investigating the effective lifetime of a Si wafer which determines the recombination rate, thus significantly affecting the voltage of a corresponding solar cell, while the contact resistance affects mostly the fill factor of the device.¹⁰ In this work, we first undertook a comparative study to examine the effect of ALD deposition temperature on the surface passivation and contact resistance of different p⁺-Si/TiO₂ samples. We note that the samples here for the lifetime tests use a symmetrical structure of TiO₂/p⁺/n/p⁺/TiO₂, allowing injection-dependent lifetime measurement with straightforward calculation of the implied voltage of the cell,¹⁰ while the samples for the p⁺-Si/TiO₂ contact test are based on a p⁺-Si/p-Si/p⁺-Si structure. By depositing a 10 nm thick TiO₂ layer at an ALD deposition temperature of 75°C, a recombination current density J₀ of 171 fA.cm⁻² can be reached. By increasing the ALD deposition temperature from 75 to 200°C, J₀ gradually increased to 470 fA.cm⁻² as shown in Fig. 1(a). Such a trend is similar to the work presented by Cui et al.,²⁰ where undiffused wafers were utilized. Based on the results reported by Aarik et al.,^{43,44} an ALD deposition temperature up to 100°C results in pure amorphous TiO₂,⁴⁵ By increasing the deposition temperature from 150°C some crystal grains appear in the structure and by further raising the temperature the structure of TiO₂ film becomes more crystalline. As the anatase phase is growing within the amorphous phase, hillocks on the film surface are formed by the crystallites which roughen the surface and also increases the surface area.^{44,46} All the aforementioned features in films deposited at temperatures above 150°C increase the recombination rate by providing more recombination sites which impact the passivation quality. Although surface passivation is deteriorated at higher temperature, the contact resistance is reduced by 300 mΩ.cm², from 580 mΩ.cm² at 75°C to 280 mΩ.cm² at 200°C (Fig. 1(b)) which favours charge transfer at the interface. This improvement in contact resistance

can be attributed to defect-mediated conductivity, where the formation of crystallites introduces some mid-gap states and grain boundaries so that these sites act as generation-recombination centres and facilitate the charge transfer.¹² Such a trade-off makes it hard to achieve excellent lifetime and low contact resistance simultaneously, a situation that we aimed to address by pre-treatment.

Hydrogen has been widely reported to be beneficial for improving the surface passivation of Si, as it can diffuse to recombination centres in the form of atomic hydrogen and deactivate them.^{10,47} A widely-established passivation approach for Si is by depositing passivation layers such as SiO₂,²⁷ Al₂O₃,⁴⁸ followed by forming gas (H₂/Ar) annealing. However, in the present work, introducing an extra passivation layer between p⁺-Si and TiO₂ using the abovementioned materials is not feasible, as it would dramatically increase the contact resistance due to their insulating nature, which necessitate having metal contact openings. Instead, in this work we introduced a novel FG pre-treatment for the Si wafer immediately before the ALD-TiO₂ deposition, and found that this simple pre-treatment enhanced the surface passivation substantially. We hypothesise that pre-treatment by FG forms hydroxyl groups on Si surface which facilitate a ligand exchange process later during the ALD deposition of TiO₂, resulting in better interaction between the Si substrate and TiO₂.³⁶ The initial surface passivation test on the boron doped silicon wafer without TiO₂ deposition revealed that FG annealing slightly improved J₀ from the initial value of 961 fA.cm⁻² for p⁺-Si to 856 fA.cm⁻² for p⁺-Si/FG, which proves that FGA is unable to passivate the silicon surface by its own, but instead it affects the following ALD deposition and enhances passivation quality. The J₀ reduction resulting from FG pre-treatment was ~40 fA.cm⁻² for ALD-TiO₂ deposited at 75°C and 100°C and ~100 fA.cm⁻², for ALD-TiO₂ deposited at 150°C, as shown in Fig 1a) The improvement is most significant for the 200°C ALD-TiO₂, with an almost threefold

reduction of J_0 from 470 fA.cm^{-2} to 152 fA.cm^{-2} (Fig 1a). Moreover the effect of TiO_2 thickness on surface passivation for a film deposited at 200°C was examined (result is presented in figure S1 in supporting information) which revealed the 10nm as the optimum thickness. The resultant improvement from FGA is stable with time; not only did the lifetime not drop after 9 weeks storage in ambient condition, but it also improved moderately (refer to figure S2 in the supporting information section). The low-temperature steady-state PL spectra demonstrated results consistent with the trends in J_0 values, with the maximum peak intensities from both the Si substrate and the p^+ layer observed for the $\text{p}^+\text{-Si/FG/TiO}_2$ sample, and intensities more than six times lower for $\text{p}^+\text{-Si}$, $\text{p}^+\text{-Si/FG}$, and $\text{p}^+\text{-Si/TiO}_2$ samples (refer to figure S3 in the supporting information and Ref⁴⁹ for the interpretation of each peak). This indicates significantly lower trap assisted recombination for both the Si substrate and the p^+ layer in the FG pre-treated samples, which can be attributed to the formation of hydrophilic hydroxyl group on the silicon surface that affect subsequent TiO_2 deposition. Meanwhile, we found such a treatment only moderately increased the contact resistance between $\text{p}^+\text{-Si}$ and TiO_2 as shown in Fig 1b), which makes it practicable to have full-area carrier selective contact. Moreover, the contact resistance is still superior to which is mentioned in the previous work for the similar structure ($2 \text{ } \Omega\text{.cm}^2$).¹² It should be noted that for perovskite/Si tandems, the issue of series resistance is much less severe relative to silicon cells (by a factor of $\sim 5^{50}$), due to the higher voltage and lower cell current, resulting from the necessity for the subcell currents to be matched. Hence, all contact resistivities obtained with the FG pre-treatment are compatible with high efficiency perovskite/Si tandem cells and the surface passivation improvement does not have to be traded off against severe resistance losses. In addition, the lateral conductivity is not so high to cause shunting.

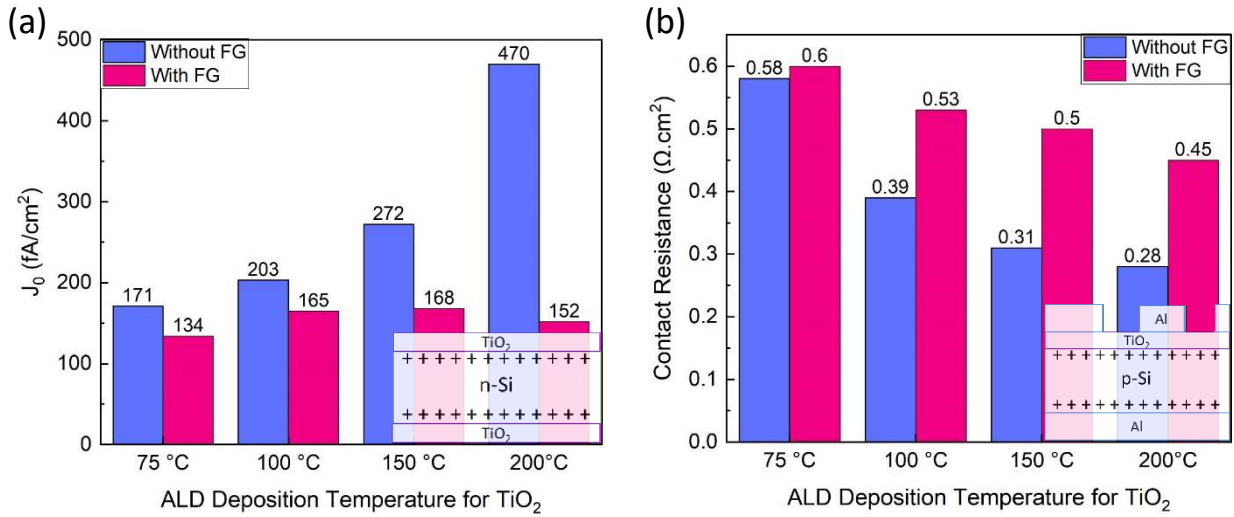


Figure 1. The effect of different ALD deposition temperature (from 75°C to 200°C) and the FG annealing pre-treatment on (a) surface passivation and (b) contact resistance with the inset sketches of the tested structures.

Some of the best Si surface passivation approaches are based on high-quality SiO₂ fabricated by high-temperature oxidation (700-1000°C).⁵¹ We therefore compared the passivation quality of our low-temperature passivation approach with these standard high-temperature passivation approaches. Based on the results, the passivation quality of samples with FG pre-treatment is comparable and even slightly better than the samples with high-temperature oxidation in our experiments (refer to figure S4 in supplementary).

The same trend of improved passivation with FG pre-treatment was observed among the samples without boron diffusion, in which FG pre-treatment enhanced the passivation quality, although with relatively lower lifetime arising from higher density of minority carriers in undoped samples, which leads to stronger impact of the surface defects on total recombination.¹⁵ We found that FG annealing resulted in a much smaller improvement for the phosphorous-diffused samples, which can be explained by the possibility of electron depletion resulting in an accumulation of holes on

the n^+ surface, resulting in a high recombination rate (refer to figure S5 in supplementary). This might indicate the presence of negative charge in the TiO_2 film²⁰ but we have been unable to confirm this hypothesis with capacitance–voltage (CV) measurements because the high conductivity of the TiO_2 results in a large current leakage.

3.2.High-resolution transmission electron microscopy (HRTEM) Analysis

In order to examine the interface layer between the silicon substrate and TiO_2 layer as well as investigating the crystallization within the TiO_2 layer, HRTEM analysis was carried out on two different samples with and without FG pre-treatment. Boron-diffused n-type samples were used with 30 minutes FG annealing at 400°C for one sample, followed by TiO_2 deposition by ALD at 200°C for both samples. TEM imaging reveals the existence of an amorphous interlayer between p^+ Si and TiO_x for both types of samples, which is a mixture of Si, Ti and O (termed as $\text{Si}_x\text{Ti}_y\text{O}_z$ here) (refer to figure S6 in supplementary). Careful analysis of the high-resolution TEM images indicates higher crystallinity of TiO_x in samples without FG in which crystal grains appear as bright features in dark field images. The density of crystallites was calculated by Gatan Digital micrograph software. While the measured density of crystallites for the sample without FG was around 0.011nm^{-2} , for the sample with FG it was almost half (0.005nm^{-2}) with mostly amorphous structure. This may be a reason for the superior surface passivation of samples with FG, since crystallization will introduce grain boundaries as extra recombination sites.¹⁰ We measured the thickness of the intermediate layer as well as the TiO_x layer in 10 different images for each condition. As can be seen from TEM images and histograms in figure 2, the average thickness of titania in samples with FG treatment is around 9.5 nm, slightly higher than without FG annealing (~8.2 nm). A possible interpretation of this trend is that samples without FG annealing contain a

hydrogen-terminated silicon bond at the surface while samples with FG have hydroxyl-terminated silicon bond in the surface. Whereas the hydrophobic nature of the former makes it difficult to adsorb the TiCl_4 precursor, the latter with a hydrophilic nature is reactive toward TiCl_4 adsorption. This would make the ligand exchange process easier between hydroxyl-terminated silicon and the gaseous precursors, resulting in higher growth rate of TiO_2 on FG annealed substrates similar to what is reported by Bent et al.³⁵ On the other hand, based on the histograms (Fig 2d), the intermediate layer in samples without FG is a little thicker (~1.3 nm compared to ~1.1 nm). The logical conclusion that can be drawn is that in ALD the initial cycles were utilized to prepare the surface bonds by making an interface layer, and for substrates without FG treatment more cycles were consumed to complete the ligand exchange process and making the intermediate layer prior to actual deposition of TiO_2 .³⁵

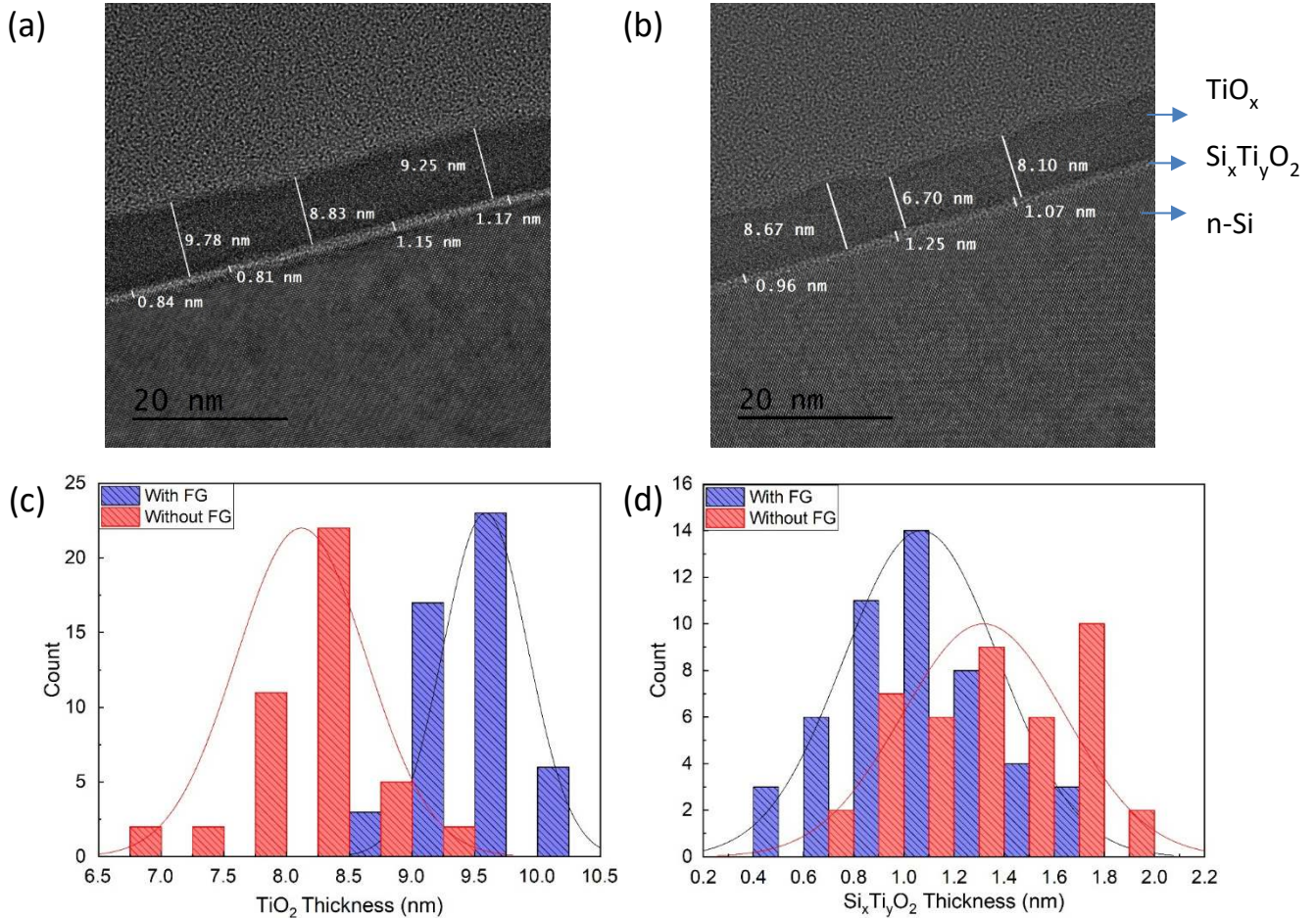


Figure 2. TEM cross section images of a) p⁺ n-Si/FG/TiO₂, b) p⁺ n-Si /TiO₂, and histogram graphs of c) TiO₂ thickness distribution, d) Si_xTi_yO₂ thickness distribution.

3.3. Effect of post-treatment

Some 2-T tandem cell architectures require a further annealing step for the perovskite top cell; for those structures it will be necessary to maintain the passivation quality of the Si cell. As the post-annealing can change the crystallization of the as-prepared TiO₂ film and thus change the interface properties, we examined the effect of post-annealing of TiO₂ layers in FG at various temperatures on phase composition, which can alter surface passivation and contact resistance. Figure 3 (a) shows that there is a gradual decrease of contact resistance and a concomitant increase in J₀ with increasing annealing temperature. Annealing at 350°C and 400°C results in dramatic

loss of the surface passivation to 540 fA/cm^2 and 620 fA/cm^2 , respectively. By making a comparison between the J_0 results and XRD patterns in figure 4b, no peaks are observed for the as-deposited TiO_2 samples as well as TiO_2 samples annealed at 250°C and 300°C , indicating low crystallization that is beyond the detection level for XRD. Upon further increasing the annealing temperature to above 350°C , peaks at 25° and 49° appear, representing the anatase phase in the (101) direction. This is the main reason for the dramatic decrease in surface passivation under these treatments, as it has been shown previously that the formation of crystal grains resulting from phase transformation from amorphous to anatase introduces grain boundaries which accelerates recombination.¹⁰ In addition, annealing the sample at temperatures above 300°C might break the Si-O-Ti bonds and form some dangling bonds,¹⁰ which could also contribute to the reduction in surface passivation. Yang et al. deposited ultra-thin layer of ALD- TiO_x with up to 5.5nm thickness on silicon substrates followed by annealing in FG for 30 minutes.²⁷ They reported that by post annealing the samples at 250°C the lifetime improved; however, a substantial passivation degradation was observed after FG annealing at temperatures $\geq 300^\circ\text{C}$. The reason for the difference between their work and the current paper can be attributed to the greater thickness of TiO_2 in our work which can accelerate the nucleation process,²⁷ and as a result no passivation enhancement is obtained even after annealing at 250°C . For the tandem structure the effect of surface passivation is more important than the contact resistance. We can estimate how much each post annealing condition will affect the performance of a 2T-tandem solar cell as follows. We used the measured contact resistance and implied V_{oc} values for each $\text{p}^+\text{-Si/TiO}_2$ condition in figure 3 (a) to estimate the tandem efficiency that would result with each structure in place of a reference structure used in our previous work.¹² Specifically, we applied the joint corrections of an adjusted V_{oc} (based on difference in iV_{oc} values between each structure and that of the reference – measured

at 606 mV) and adjusted series resistance (again compared to the reference contact resistivity of $2 \Omega \cdot \text{cm}^2$) to correct the reference tandem's IV curve and thereby obtain an estimated efficiency value. Figure S7a) in the supporting information section shows this increment in (absolute) efficiency relative to the reference for each structure. Based on the obtained results for samples without post annealing, the absolute efficiency could improve by about 0.86% compared to the reference cell with 3.5% Voc enhancement. Post annealing at 250°C, 300°C, 350°C, and 400°C would increase the efficiency of the tandem cell in comparison with the reference cell by around 0.87%, 0.74%, 0.42%, and 0.26%, respectively. Also, the J-V curve for the TiO₂/Si contact in various samples without and with post annealing of TiO₂, is presented in figure S7b) in the supporting information section that displays conductive but nonlinear J-V behavior.

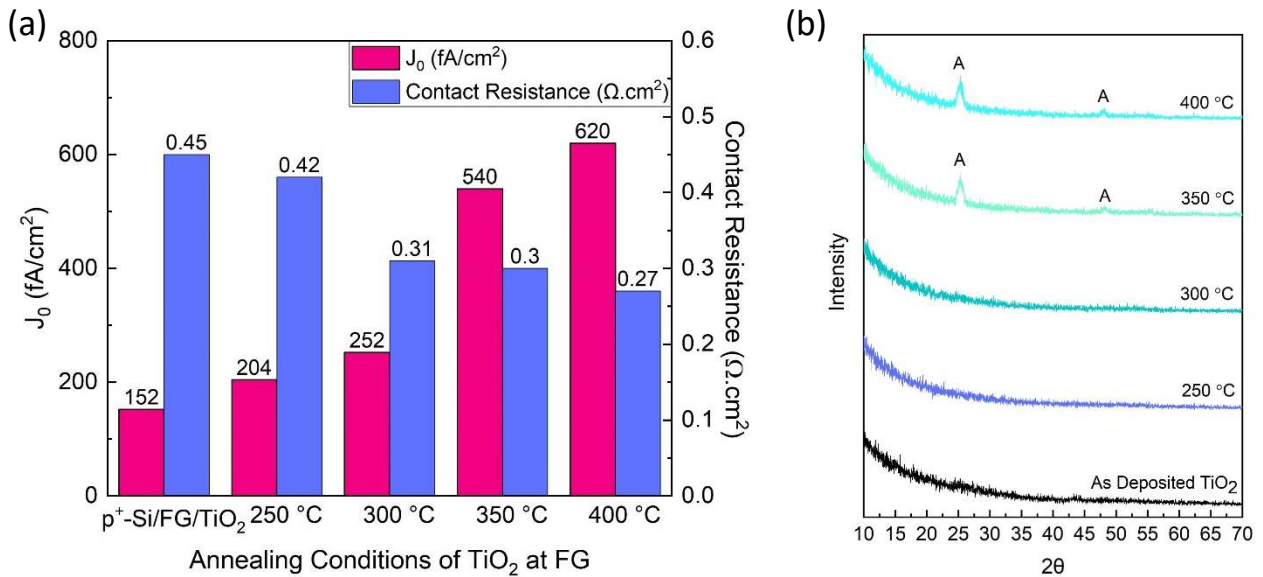


Figure 3. (a) The effect of post annealing temperature on surface passivation and contact resistance for the TiO₂ layer deposited at 200°C, (b) the corresponding XRD pattern for TiO₂ different annealing temperatures (A = anatase).

3.4. X-ray Photoelectron Spectroscopy and Ultraviolet photoelectron spectroscopy Analysis

To determine elemental composition, chemical state, electronic state, and binding energy, X-ray Photoelectron Spectroscopy (XPS) was carried out. Due to the XPS measurement depth of ~10 nm, different samples with different thicknesses were fabricated to supply information from both interface and the bulk of TiO₂. Moreover, in order to investigate the electronic characteristics of the samples including work function and energy level structure, ultraviolet photoelectron spectroscopy (UPS) was utilized. UPS provides information of how FG annealing can alter the work function and electronic structure in the valence electron region. Fig 4. plots the XPS result for 2p orbitals of Si and Ti for TiO₂ deposited on boron doped n-Si samples with different thicknesses of TiO₂ for an ALD deposition temperature of 200°C, as with 10nm TiO₂ on Si surface, the Si was not observable from XPS thus not plotted in the figure 4 (a). There are four different peaks in the Si 2p fitting diagram representing Si-Si, SiO_x-Si, Si-O/Si-O-Ti (compatible),^{52,53} and O-Si-O^{54,55} bonds with around 99.1, 100.2, 101.8, and 103.0 eV (± 0.2 eV) binding energies,^{35,52,56,57} respectively. It needs to be pointed out that such peaks represent a range of different oxidation states of Si, depending on its crystallite geometry with O bond incorporated. The Si binding energy increases with increasing Si oxidation state.^{58,59} While the Si-Si peak is present for all samples, the other three peaks are only apparent in some of them. Although for the p⁺-Si sample the only visible peak is Si-Si, FG annealing introduces O-Si-O bond (p⁺-Si/FG). The presence of the 103.0eV Si peak after FG annealing indicating an O-Si-O species is compatible with the formation of ultra-thin hydroxyl-enriched SiO₂ as proposed by Hu & Turner.³⁶ It can be seen that for samples with FG pre-treatment, for 1.5nm thickness of TiO₂ the peak of O-Si-O is very small but becomes more intense when the TiO₂ thickness is increased to 6nm. Also SiO_x-Si and Si-O peaks that were absent for the thinner film, can be seen for the thicker one. It should be

noted that the 101.8eV peak assigned to Si-O is also compatible with assigning to Si-O-Ti.^{54,35} Occurrence of the SiO_x-Si and Si-O peaks can be explained by the higher amount of available oxygen in the titania layer that can be used by the Si substrate to make an oxide layer in between. For samples without FG pre-treatment for 1.5nm thickness of TiO₂ there is a very small peak of O-Si-O with no Si-O/Si-O-Ti (compatible) and SiO_x-Si peaks (quantified results are presented in table S1 in supporting information section). However, for 6nm TiO₂ the peak intensity for Si-O/Si-O-Ti (compatible) is slightly increased. The possible reason for the lower intensity of this peak might be the hydrophobic nature of this silicon substrate which slows down the formation of the Si-O-Ti bond.³⁵ For samples with annealed TiO₂ (at 300°C, FG) a similar trend can be observed in which the O-Si-O peak is smaller for the 1.5nm sample compared with the 6nm sample, and in addition the Si-O (identification compatible with Si-O-Ti) peak also appears in the sample containing 6nm TiO₂. The existence of these two peaks is possibly an indication for the formation of an oxide layer at the interface at the expense of a reduction of TiO_x.

Fig. 4 (b) shows the Ti 2p fitting with four different peak positions comprising Ti³⁺(TiO_x/Ti-O-Si)⁶⁰ and Ti⁴⁺(TiO₂)⁶¹ peaks corresponding to Ti 2p_{3/2} orbital located at around 457.5 and 459.4eV,⁶² respectively. Ti⁴⁺ peaks for both orbitals are present in all conditions. For samples with FG pre-treatment it can be seen that by increasing the thickness of TiO₂ from 1.5nm to 6nm, the peak intensity of Ti³⁺ decreased which can be attributed to the Ti-O-Si bond that is related to the interface and is getting hard to detect as the TiO₂ is becoming thicker. The intensity of the Ti peak is thus attributed mostly to the TiO₂ bulk. For samples without FG pre-treatment and samples with pre-treatment and post FG annealing of TiO₂ at 300°C, higher intensity for the Ti³⁺ peak was observed by comparison with the analogous sample with FG pre-treatment (quantified results are presented in table S2 in supporting information section). Ti³⁺ defects are recombination sites which

deteriorate passivation and increase J_0 at the interface, and can be found in the bulk as well as the interface of TiO_2 . Based on previous papers one hypothesis is that defects available on the substrate surface plus the temperature during annealing can provide enough activation energy for H_2 molecules to be dissociated into H atoms and penetrate into the surface which later after exposure to oxygen can form hydroxyl group on the surface.^{47,63} By post annealing of TiO_2 , Ti loses some of its oxygen and transforms to lower oxidation states (Ti^{3+}) which can makes some sub-bandgap states and introduces new recombination sites.³⁵ We note that the Ti^{4+} showed slight shift to a lower binding energy of 6nm TiO_2 samples. This could be due to the different ALD processing batch of various thicknesses. Since the Ti^{4+} and Ti^{3+} peaks were still observable, such a shift would not affect the fitting of the XP spectra.⁶⁴

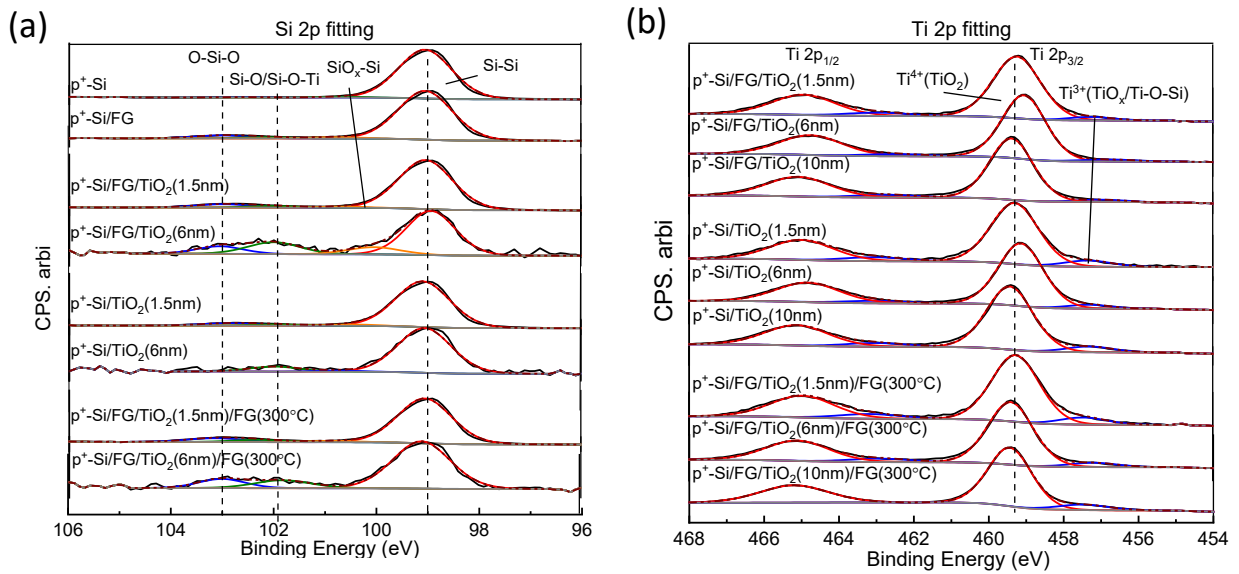


Figure 4. XPS result for (a) Si 2p, (b) Ti 2p orbitals for p⁺ n-Si/TiO₂ samples with different TiO₂ thicknesses.

Figure 5 depicts the density of states (DOS) of valence electron close to the Fermi level for p^+ -Si/TiO₂(10nm), p^+ -Si/FG/TiO₂(10nm), and p^+ -Si/FG/TiO₂(10nm)/FG(300°C) . As can be seen from the graph in the range of 1.5 eV - 0eV binding energy, the sample without FG pre-treatment has a higher DOS of electrons at lower binding energy arising from the formation of lower electronegativity cations and surface dipole change which give rise to the work function reduction.⁶⁵ In light of the higher density of low-oxidation-state cation (Ti³⁺) among all samples without FG pre-treatment compared with their equivalent sample with FG pre-treatment (Fig.5), it could be argued that O-vacancy defects available within the bulk and interface of TiO₂ are responsible for higher recombination rate in these samples.^{65,66} By applying the FG annealing to the p^+ -Si/FG/TiO₂ sample (red line in figure 5), the DOS for electrons with low binding energy decreased (evident by the decrease in Ti³⁺ defect states close to the Fermi level). Post annealing of the TiO_x layer at FG at 300°C increased the DOS within the range of 1.5 eV-0eV binding energy. Post annealing provides some activation energy for titania reduction which introduces some unpaired electrons in the valence band of Ti with low binding energy which leads to an increase in the DOS for these electrons followed by improving the contact in this sample. The electronic characterization indicated that FG pre-treatment slightly shifted conduction and valence energy level upwards (refer to figure S8 in supplementary), which enlarged the band offset between the TiO₂ conduction band edge and the Si valence band (Δ) from 0.4eV in the sample without FG pre-treatment to 0.45eV in the sample with FG. Moreover, after post annealing of TiO₂ in FG the energy levels showed a downward shift that decreased the Δ factor to 0.35eV. It is well-known that the band offset is one of the responsible factors affecting the conductivity between TiO₂ and p^+ -Si.¹² This influence on the conductivity is not compensated by the increase in DOS close to the Fermi level due to the increase in Ti³⁺ defect states. Therefore the obtained results are consistent

with the contact resistance measurements in which the contact resistance was slightly better for the sample without FG and also it improved after post annealing of the sample with FG pre-treatment (refer to figure 3(a)). In summary XPS and UPS results demonstrate the positive effect of FG pre-treatment in improving the passivation of the Si substrate by decreasing the defect density at interface between the Si and TiO₂ layer and upward shifting of the energy states of the TiO₂ layer.

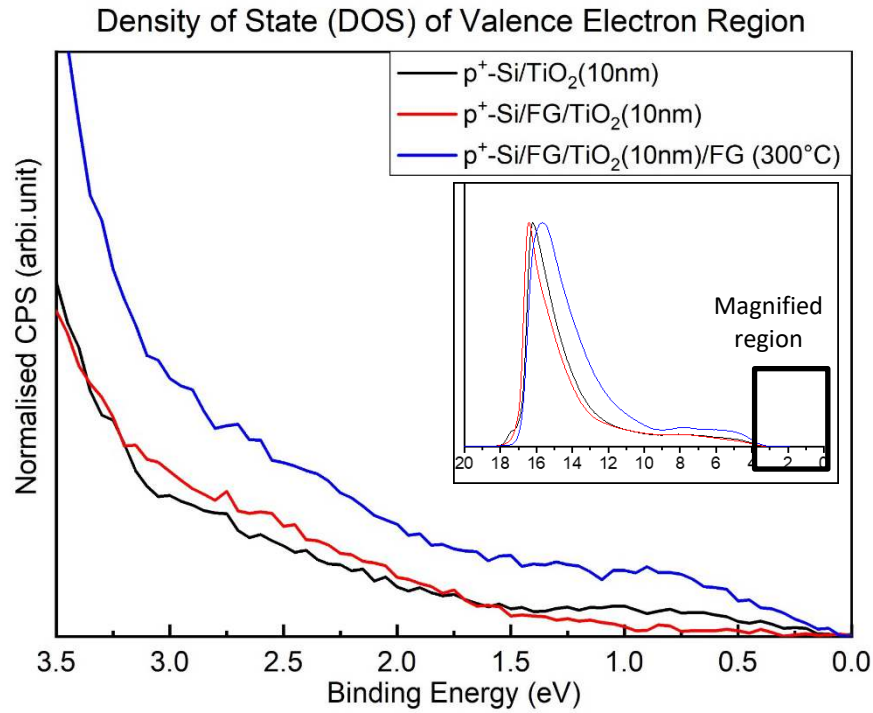


Figure 5. Density of states of valance electrons for different samples. The energy ranging from 0 to 3.5eV is magnified.

4. Conclusion

In this study we demonstrated the excellent performance of a FG pre-treatment (400°C, 30 min) in combination with ALD-TiO₂ as a passivation and potential carrier selective contact layer for

highly boron doped silicon of $23 \text{ } \Omega/\text{sq}$. With this combined treatment we achieved a J_0 of $152 \text{ fA}\cdot\text{cm}^{-2}$ and a contact resistance of $0.45 \Omega\text{cm}^2$ for ALD- TiO_2 deposited at 200°C . This low contact resistance eliminates further need for localized contact structures. The comparison between different ALD deposition temperatures shows a significant improvement in Si surface passivation when including the FG pre-treatment irrespective of the TiO_2 deposition temperature. The FG pre-treatment significantly improves surface passivation without a strong increase in contact resistance. Furthermore, the passivation quality of the best FG pre-treated TiO_2 films exceeds that of thermally-grown SiO_2 (700°C). HRTEM characterisation showed higher crystallinity for samples without FG pre-treatment, which is one reason for the inferior passivation quality of these samples. The results of XRD measurements show that the TiO_2 samples with FG pre-treatment were nearly completely amorphous. XPS results confirmed the almost stoichiometric composition of TiO_2 with a lower density of defects for samples with FG pre-treatment which explains the superior passivation of these samples. We hypothesise that the pre-treatment in FG forms an ultrathin interfacial silicon oxide terminated with hydroxyl groups that facilitates the immediate chemisorption of the TiCl_4 precursor and thereby stoichiometric, defect-lean TiO_2 deposition without delay (no incubation cycles). Also, the H_2 molecules in the forming gas can dissociate into atomic hydrogen and passivate defects on the surface. The FG pre-treatment represents a novel, useful, and easy method to increase the passivation quality of the c-Si wafers by ALD- TiO_x with application potential in both perovskite/Si tandems and single-junction Si solar cells.

ASSOCIATED CONTENT

Supporting Information

The supporting information is available free of charge. It comprises experimental details, additional figures including the effect of TiO₂ thickness, stability test, PL spectra, the effect of various pre-heat treatment conditions, the passivation results for samples without boron diffusion and with phosphorous diffusion, elemental map, the simulation result, energy level structure, plus tables including relative intensity of Si species, and Ti³⁺ defect rate.

AUTHOR INFORMATION

Corresponding Authors

*Email: kylie.catchpole@anu.edu.au

*Email: naeimeh.mozaffari@anu.edu.au

Author Contributions

The manuscript was written through contributions of all authors. All authors have given approval to the final version of the manuscript.

Notes

The authors declare no conflict of interest

ACKNOWLEDGMENT

We acknowledge the support of the Australian Renewable Energy Agency (ARENA), the Australian Centre for Advanced Photovoltaics (ACAP), and the ANFF ACT Node in carrying out this research. H.T.N. acknowledges the fellowship support of the Australian Centre for Advanced Photovoltaics. T. W. is the recipient of an Australian Research Council Future Fellowship (project number FT180100302) funded by the Australian Government.

REFERENCES

- (1) Liao, B.; Hoex, B.; Aberle, A. G.; Chi, D.; Bhatia, C. S. Excellent C-Si Surface Passivation by Low-Temperature Atomic Layer Deposited Titanium Oxide. *Appl. Phys. Lett.* **2014**, *104* (25), 253903.
- (2) Cuevas, A.; Wan, Y.; Yan, D.; Samundsett, C.; Allen, T.; Zhang, X.; Cui, J.; Bullock, J. Carrier Population Control and Surface Passivation in Solar Cells. *Sol. Energy Mater. Sol. Cells* **2018**, *184*, 38–47.
- (3) Titova, V.; Veith-Wolf, B.; Startsev, D.; Schmidt, J. Effective Passivation of Crystalline Silicon Surfaces by Ultrathin Atomic-Layer-Deposited TiO_x layers. *Energy Procedia* **2017**, *124*, 441–447.
- (4) Aberle, A. G. Surface Passivation of Crystalline Silicon Solar Cells: A Review. *Prog. Photovoltaics Res. Appl.* **2000**, *8* (5), 473–487.
- (5) Aberle, A. G.; Glunz, S.; Warta, W. Field Effect Passivation of High Efficiency Silicon Solar Cells. *Sol. Energy Mater. Sol. Cells* **1993**, *29* (2), 175–182.
- (6) Kho, T. C.; Fong, K.; McIntosh, K.; Franklin, E.; Grant, N.; Stocks, M.; Phang, S. P.; Wan, Y.; Wang, E. C.; Vora, K.; Ngwe, Z.; Blakers, A. Exceptional Silicon Surface Passivation by an ONO Dielectric Stack. *Sol. Energy Mater. Sol. Cells* **2018**, *189*, 245–253.
- (7) Wu, Y.; Yan, D.; Peng, J.; Duong, T.; Wan, Y.; Phang, S. P.; Shen, H.; Wu, N.; Barugkin, C.; Fu, X.; Surve, S.; Grant, D.; Walter, D.; White, T. P.; Catchpole, K. R.; Weber, K. J. Monolithic Perovskite/Silicon-Homojunction Tandem Solar Cell with over 22% Efficiency. *Energy Environ. Sci.* **2017**, *10*, 2472–2479.

- (8) Adachi, D.; Hernández, J. L.; Yamamoto, K. Impact of Carrier Recombination on Fill Factor for Large Area Heterojunction Crystalline Silicon Solar Cell with 25.1% Efficiency. *Appl. Phys. Lett.* **2015**, *107* (23), 233506.
- (9) Moldovan, A.; Feldmann, F.; Zimmer, M.; Rentsch, J.; Benick, J.; Hermle, M. Tunnel Oxide Passivated Carrier-Selective Contacts Based on Ultra-Thin SiO₂ Layers. *IEEE 42nd Photovolt. Spec. Conf.* **2015**, 1–6.
- (10) Yang, X.; Bi, Q.; Ali, H.; Davis, K.; Schoenfeld, W. V.; Weber, K. High-Performance TiO₂-Based Electron-Selective Contacts for Crystalline Silicon Solar Cells. *Adv. Mater.* **2016**, *28* (28), 5891–5897.
- (11) Bush, K. A.; Palmstrom, A. F.; Yu, Z. J.; Boccard, M.; Cheacharoen, R.; Mailoa, J. P.; McMeekin, D. P.; Hoye, R. L. Z.; Bailie, C. D.; Leijtens, T.; Peters, I. M.; Minichetti, M. C.; Rolston, N.; Prasanna, R.; Sofia, S.; Harwood, D.; Ma, W.; Moghadam, F.; Snaith, H. J.; Buonassisi, T.; Holman, Z. C.; Bent, S. F.; McGehee, M. D. 23.6%-Efficient Monolithic Perovskite/Silicon Tandem Solar Cells With Improved Stability. *Nat. Energy* **2017**, *2* (4), 1–7.
- (12) Shen, H.; Omelchenko, S. T.; Jacobs, D. A.; Yalamanchili, S.; Wan, Y.; Yan, D.; Phang, P.; Duong, T.; Wu, Y.; Yin, Y.; Samundsett, C.; Peng, J.; Wu, N.; White, T. P.; Andersson, G. G.; Lewis, N. S.; Catchpole, K. R. In Situ Recombination Junction between P-Si and TiO₂ Enables High-Efficiency Monolithic Perovskite/Si Tandem Cells. *Sci. Adv.* **2018**, *4* (12), 1–21.
- (13) Zheng, J.; Lau, C. F. J.; Mehrvarz, H.; Ma, F. J.; Jiang, Y.; Deng, X.; Soeriyadi, A.; Kim, J.; Zhang, M.; Hu, L.; Cui, X.; Lee, D. S.; Bing, J.; Cho, Y.; Chen, C.; Green, M. A.; Huang,

- S.; Ho-Baillie, A. W. Y. Large Area Efficient Interface Layer Free Monolithic Perovskite/Homo-Junction-Silicon Tandem Solar Cell with over 20% Efficiency. *Energy Environ. Sci.* **2018**, *11* (9), 2432–2443.
- (14) Green, M. A. Commercial Progress and Challenges for Photovoltaics. *Nat. Energy* **2016**, *1* (1), 1–4.
- (15) Aberle, A. G. Crystalline Silicon Solar Cells: A Review. *Prog. Photovolt Res. Appl.* **2000**, *8* (May), 473–487.
- (16) Benick, J.; Hoex, B.; Van De Sanden, M. C. M.; Kessels, W. M. M.; Schultz, O.; Glunz, S. W. High Efficiency N-Type Si Solar Cells on Al₂O₃-Passivated Boron Emitters. *Appl. Phys. Lett.* **2008**, *92* (25), 253504.
- (17) Mihailetschi, V. D.; Komatsu, Y.; Geerligs, L. J. Nitric Acid Pretreatment for the Passivation of Boron Emitters for n -Type Base Silicon Solar Cells. *Appl. Phys. Lett.* **2008**, *92* (6), 14–17.
- (18) Bullock, J.; Yan, D.; Wan, Y.; Cuevas, A.; Demareux, B.; Hessler-Wyser, A.; De Wolf, S. Amorphous Silicon Passivated Contacts for Diffused Junction Silicon Solar Cells. *J. Appl. Phys.* **2014**, *115* (16), 163703.
- (19) Hoex, B.; Schmidt, J.; Bock, R.; Altermatt, P. P.; Van De Sanden, M. C. M.; Kessels, W. M. M. Excellent Passivation of Highly Doped p -Type Si Surfaces by the Negative-Charge-Dielectric Al₂O₃. *Appl. Phys. Lett.* **2007**, *91* (11), 1–4.
- (20) Cui, J.; Allen, T.; Wan, Y.; Mckee, J.; Samundsett, C.; Yan, D.; Zhang, X.; Cui, Y.; Chen, Y.; Verlinden, P.; Cuevas, A. Titanium Oxide: A Re-Emerging Optical and Passivating

- Material for Silicon Solar Cells. *Sol. Energy Mater. Sol. Cells* **2016**, *158*, 115–121.
- (21) Lin, F.; Hoex, B.; Koh, Y. H.; Lin, J. J.; Aberle, A. G. Low-Temperature Surface Passivation of Moderately Doped Crystalline Silicon by Atomic-Layer-Deposited Hafnium Oxide Films. *ECS J. Solid State Sci. Technol.* **2013**, *2* (1), N11–N14.
- (22) Wan, Y.; Bullock, J.; Cuevas, A. Passivation of C-Si Surfaces by ALD Tantalum Oxide Capped with PECVD Silicon Nitride. *Sol. Energy Mater. Sol. Cells* **2015**, *142*, 42–46.
- (23) Allen, T. G.; Cuevas, A. Electronic Passivation of Silicon Surfaces by Thin Films of Atomic Layer Deposited Gallium Oxide. *Appl. Phys. Lett.* **2014**, *105* (3), 031601.
- (24) Saint-Cast, P.; Richter, A.; Billot, E.; Hofmann, M.; Benick, J.; Rentsch, J.; Preu, R.; Glunz, S. W. Very Low Surface Recombination Velocity of Boron Doped Emitter Passivated with Plasma-Enhanced Chemical-Vapor-Deposited AlO_x Layers. *Thin Solid Films* **2012**, *522*, 336–339.
- (25) Krugel, G.; Sharma, A.; Wolke, W.; Rentsch, J.; Preu, R. Study of Hydrogenated AlN as an Anti-Reflective Coating and for the Effective Surface Passivation of Silicon. *Phys. Status Solidi - Rapid Res. Lett.* **2013**, *7* (7), 457–460.
- (26) Schmidt, J.; Veith, B.; Brendel, R. Effective Surface Passivation of Crystalline Silicon Using Ultrathin Al₂O₃ Films and Al₂O₃/SiN_x Stacks. *Phys. Status Solidi - Rapid Res. Lett.* **2009**, *3* (9), 287–289.
- (27) Yang, X.; Zheng, P.; Bi, Q.; Weber, K. Silicon Heterojunction Solar Cells with Electron Selective TiO_xcontact. *Sol. Energy Mater. Sol. Cells* **2016**, *150*, 32–38.
- (28) Yang, X.; Weber, K.; Hameiri, Z.; Wolf, S. De. Industrially Feasible, Dopant-free, Carrier-

- selective Contacts for High-efficiency Silicon Solar Cells. *Prog. Photovoltaics* **2017**, No. 25, 896–904.
- (29) Cahill, D. G.; Allen, T. H. Thermal Conductivity of Sputtered and Evaporated SiO₂ and TiO₂ Optical Coatings. *Appl. Phys. Lett.* **1994**, *65* (3), 309–311.
- (30) Richards, B. S.; Cotter, J. E.; Honsberg, C. B. Enhancing the Surface Passivation of TiO₂ Coated Silicon Wafers. *Appl. Phys. Lett.* **2002**, *80* (7), 1123–1125.
- (31) Barbé, J.; Thomson, A. F.; Wang, E. C.; McIntosh, K.; Catchpole, K. Nanoimprinted TiO₂ Sol-Gel Passivating Diffraction Gratings for Solar Cell Applications. *Prog. Photovoltaics Res. Appl.* **2012**, *20* (2), 143–148.
- (32) Wang, Z.; Yao, N.; Hu, X. Single Material TiO₂ Double Layers Antireflection Coating with Photocatalytic Property Prepared by Magnetron Sputtering Technique. *Vacuum* **2014**, *108*, 20–26.
- (33) Thomson, A. F.; McIntosh, K. R. Light-Enhanced Surface Passivation of TiO₂-Coated Silicon. *Prog. Photovoltaics Res. Appl.* **2012**, *20* (3), 343–349.
- (34) Liao, B.; Hoex, B.; Shetty, K. D.; Basu, P. K.; Bhatia, C. S. Passivation of Boron-Doped Industrial Silicon Emitters by Thermal Atomic Layer Deposited Titanium Oxide. *IEEE J. Photovoltaics* **2015**, *5* (4), 1062–1066.
- (35) Methaapanon, R.; Bent, S. F. Comparative Study of Titanium Dioxide Atomic Layer Deposition on Silicon Dioxide and Hydrogen-Terminated Silicon. *J. Phys. Chem. C* **2010**, *114* (23), 10498–10504.
- (36) Hu, Z.; Turner, C. H. Initial Surface Reactions of TiO₂ Atomic Layer Deposition onto SiO₂

- Surfaces: Density Functional Theory Calculations. *J. Phys. Chem. B* **2006**, *110* (16), 8337–8347.
- (37) Kern, W. The Evolution of Silicon Wafer Cleaning Technology. *J. Electrochem. Soc.* **1990**, *137* (6), 1887–1892.
- (38) Cuevas, A.; Macdonald, D. Measuring and Interpreting the Lifetime of Silicon Wafers. *Sol. Energy* **2004**, *76* (1–3), 255–262.
- (39) Nguyen, H. T.; Baker-Finch, S. C.; MacDonald, D. Temperature Dependence of the Radiative Recombination Coefficient in Crystalline Silicon from Spectral Photoluminescence. *Appl. Phys. Lett.* **2014**, *104* (11), 112105.
- (40) Cox, R. H.; Strack, H. Ohmic Contacts for GaAs Devices. *Solid. State. Electron.* **1967**, *10* (12), 1213–1218.
- (41) Acres, R. G.; Ellis, A. V.; Alvino, J.; Lenahan, C. E.; Khodakov, D. A.; Metha, G. F.; Andersson, G. G. Molecular Structure of 3-Aminopropyltriethoxysilane Layers Formed on Silanol-Terminated Silicon Surfaces. *J. Phys. Chem. C* **2012**, *116* (10), 6289–6297.
- (42) Yin, Y.; Sibley, A.; Quinton, J. S.; Lewis, D. A.; Andersson, G. G. Dipole Formation at the MoO₃/Conjugated Polymer Interface. *Adv. Funct. Mater.* **2018**, *28* (46), 1–10.
- (43) Uustare, T.; Aarik, J.; Aidla, A.; Ma, H. Atomic Layer Deposition of Titanium Dioxide from TiCl₄ and H₂O : Investigation of Growth Mechanism. *Appl. Surf. Sci.* **2001**, *172*, 148–158.
- (44) Aarik, J.; Aidla, A.; Mändar, H.; Sammelselg, V. Anomalous Effect of Temperature on Atomic Layer Deposition of Titanium Dioxide. *J. Cryst. Growth* **2000**, *220* (4), 531–537.

- (45) Aarik, J.; Aidla, A.; Kiisler, A. A.; Uustare, T.; Sammelseg, V. Effect of Crystal Structure on Optical Properties of TiO₂ Films Grown by Atomic Layer Deposition. *Thin Solid Films* **1997**, *305* (1–2), 270–273.
- (46) Chiappim, W.; Testoni, G. E.; Moraes, R. S.; Pessoa, R. S.; Sagás, J. C.; Origo, F. D.; Vieira, L.; MacIel, H. S. Structural, Morphological, and Optical Properties of TiO₂ Thin Films Grown by Atomic Layer Deposition on Fluorine Doped Tin Oxide Conductive Glass. *Vacuum* **2016**, *123*, 91–102.
- (47) Sopori, B. L.; Deng, X.; Benner, J. P.; Rohatgi, A.; Sana, P.; Estreicher, S. K.; Park, Y. K.; Roberson, M. A. Hydrogen in Silicon: A Discussion of Diffusion and Passivation Mechanisms. *Sol. Energy Mater. Sol. Cells* **1996**, *41–42*, 159–169.
- (48) Suh, D.; Choi, D.-Y.; Weber, K. J. Al₂O₃ /TiO₂ Stack Layers for Effective Surface Passivation of Crystalline Silicon. *J. Appl. Phys.* **2013**, *114* (15), 154107.
- (49) Nguyen, H. T.; Yan, D.; Wang, F.; Zheng, P.; Han, Y.; Macdonald, D. Micro-Photoluminescence Spectroscopy on Heavily-Doped Layers of Silicon Solar Cells. *Phys. Status Solidi - Rapid Res. Lett.* **2015**, *9* (4), 230–235.
- (50) Werner, J.; Niesen, B.; Ballif, C. Perovskite/Silicon Tandem Solar Cells: Marriage of Convenience or True Love Story? – An Overview. *Adv. Mater. Interfaces* **2018**, *5* (1), 1–19.
- (51) Glunz, S. W.; Feldmann, F. SiO₂ Surface Passivation Layers – a Key Technology for Silicon Solar Cells. *Sol. Energy Mater. Sol. Cells* **2018**, *185* (February), 260–269.
- (52) Dwivedi, N.; Yeo, R. J.; Tan, H. R.; Stangl, R.; Aberle, A. G.; Bhatia, C. S.; Danner, A.;

- Liao, B. Evidence for Chemicals Intermingling at Silicon/Titanium Oxide (TiO_x) Interface and Existence of Multiple Bonding States in Monolithic TiO_x . *Adv. Funct. Mater.* **2018**, 28 (28), 1707018.
- (53) Sublemontier, O.; Nicolas, C.; Aureau, D.; Patanen, M.; Kintz, H.; Liu, X.; Gaveau, M. A.; Le Garrec, J. L.; Robert, E.; Barreda, F. A.; Etcheberry, A.; Reynaud, C.; Mitchell, J. B.; Miron, C. X-Ray Photoelectron Spectroscopy of Isolated Nanoparticles. *J. Phys. Chem. Lett.* **2014**, 5 (19), 3399-3403.
- (54) Jensen, D. S.; Kanyal, S. S.; Madaan, N.; Vail, M. A.; Dadson, A. E.; Engelhard, M. H.; Linford, M. R. Silicon (100)/ SiO_2 by XPS. *Surf. Sci. Spectra* **2013**, 20 (1), 36–42.
- (55) Larina, T. V.; Dovlitova, L. S.; Kaichev, V. V.; Malakhov, V. V.; Glazneva, T. S.; Paukshtis, E. A.; Bal'Zhinimaev, B. S. Influence of the Surface Layer of Hydrated Silicon on the Stabilization of Co^{2+} Cations in Zr-Si Fiberglass Materials According to XPS, UV-Vis DRS, and Differential Dissolution Phase Analysis. *RSC Adv.* **2015**, 5 (97), 79898–79905.
- (56) Brassard, D.; Sarkar, D. K.; El Khakani, M. A.; Quellet, L. Tuning the Electrical Resistivity of Pulsed Laser Deposited TiSiO_x Thin Films from Highly Insulating to Conductive Behaviors. *Appl. Phys. Lett.* **2004**, 84 (13), 2304–2306.
- (57) Zhong, N.; Shima, H.; Akinaga, H. Mechanism of the Performance Improvement of TiO_2 - x -Based Field-Effect Transistor Using SiO_2 as Gate Insulator. *AIP Adv.* **2011**, 1 (3), 032167.
- (58) Arezzo, F.; Severini, E.; Zacchetti, N. An XPS Study of Diamond Films Grown on Differently Pretreated Silicon Substrates. *Surf. Interface Anal.* **1994**, 22 (1-12), 218–223.

- (59) Aarnink, W. A. M.; Weishaupt, A.; van Silfhout, A. Angle-Resolved X-Ray Photoelectron Spectroscopy (ARXPS) and a Modified Levenberg-Marquardt Fit Procedure: A New Combination for Modeling Thin Layers. *Appl. Surf. Sci.* **1990**, *45* (1), 37–48.
- (60) Krishnan, G.; Al Qahtani, H. S.; Li, J.; Yin, Y.; Eom, N.; Golovko, V. B.; Metha, G. F.; Andersson, G. G. Investigation of Ligand-Stabilized Gold Clusters on Defect-Rich Titania. *J. Phys. Chem. C* **2017**, *121* (50), 28007–28016.
- (61) Jin, C.; Liu, B.; Lei, Z.; Sun, J. Structure and Photoluminescence of the TiO₂ Films Grown by Atomic Layer Deposition Using Tetrakis-Dimethylamino Titanium and Ozone. *Nanoscale Res. Lett.* **2015**, *10* (1), 1–9.
- (62) Netterfield, R. P.; Martin, P. J.; Pacey, C. G.; Sainty, W. G.; McKenzie, D. R.; Auchterlonie, G. Ion-Assisted Deposition of Mixed TiO₂-SiO₂ Films. *J. Appl. Phys.* **1989**, *66* (4), 1805–1809.
- (63) Kisielowski-Kemmerich, C.; Beyer, W. Hydrogen Desorption from Crystalline Silicon and Its Modification Due to the Presence of Dislocations. *J. Appl. Phys.* **1989**, *66* (2), 552–558.
- (64) Such error bar was calculated based on hemispherical electron energy analyser resolution and uncertainty in the fitting procedure. The former one was calculated from electron pass energy and hemisphere path length. The latter one was processed from the di, a fitting region based on peak cut-off of X. was considered as minimum fitting region while a fitting region based on absolute base line was regarded as maximum fitting region.
- (65) Greiner, M. T.; Chai, L.; Helander, M. G.; Tang, W. M.; Lu, Z. H. Transition Metal Oxide Work Functions: The Influence of Cation Oxidation State and Oxygen Vacancies. *Adv.*

Funct. Mater. **2012**, 22 (21), 4557–4568.

- (66) Pan, S.; Liu, X.; Guo, M.; Yu, S. F.; Huang, H.; Fan, H.; Li, G. Engineering the Intermediate Band States in Amorphous Ti³⁺-Doped TiO₂ for Hybrid Dye-Sensitized Solar Cell Applications. *J. Mater. Chem. A* **2015**, 3 (21), 11437–11443.

Table of Contents (TOC) graphic

